

Best Practices in Utilization of 2D-NMR Spectral Data as the Input for Chemometric Analysis in Biopharmaceutical Applications

Robert G. Brinson,* Luke W. Arbogast, John P. Marino, and Frank Delaglio



Cite This: <https://dx.doi.org/10.1021/acs.jcim.0c00081>



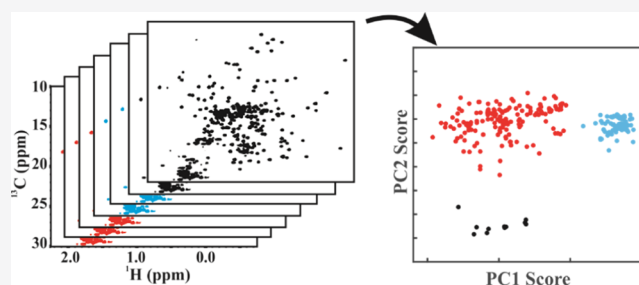
Read Online

ACCESS |

Metrics & More

Article Recommendations

ABSTRACT: Quality attributes (QAs) are measurable parameters of a biologic that impact product safety and efficacy and are essential characteristics that are linked to positive patient health outcomes. One QA, higher order structure (HOS), is directly coupled to the function of protein biologics, and deviations in this QA may cause adverse effects. To address the critical need for HOS assessment, methods for analyzing structural fingerprints from 2D nuclear magnetic resonance spectroscopy (2D-NMR) spectra have been established for drug substances as large as monoclonal antibody therapeutics. Here, chemometric analyses have been applied to 2D ^1H , ^{13}C -methyl NMR correlation spectra of the IgG1 κ NIST monoclonal antibody (NISTmAb), recorded at natural isotopic abundance, to benchmark the performance and robustness of the methods. In particular, a variety of possible spectral input schemes (e.g., chemical shift, peak intensity, and total spectral matrix) into chemometric algorithms are examined using two case studies: (1) a large global 2D-NMR interlaboratory study and (2) a blended series of enzymatically glycan-remodeled NISTmAb isoforms. These case studies demonstrate that the performance of chemometric algorithms using either peak positions or total spectral matrix as the input will depend on the study design and likely be product-specific. In general, peak positions are found to be a more robust spectral parameter for input into chemometric algorithms, whereas the total spectral matrix approach lends itself to easier automation and requires less user intervention. Analysis with different input data also shows differences in sensitivity to certain changes in HOS, highlighting that product knowledge will further guide appropriate method selection based on the fit-for-purpose application in the context of biopharmaceutical development, production, and quality control.



1. INTRODUCTION

Statistical analyses applied to 1D-nuclear magnetic resonance (NMR) spectral data have seen tremendous growth in the fields of metabolomics, metabonomics, and complex mixture analysis.^{1–3} In contrast, 2D-NMR homo- and hetero-nuclear spectra have been used less often, owing to greater measurement requirements for data acquisition as well as greater complexity required in data handling.^{4,5} Within biomolecular NMR, applications of chemometrics have been utilized in some niche areas such as ligand binding,^{6–8} protein folding,⁹ conformational analysis,¹⁰ and allosteric networks.¹¹

Statistical analysis in the field of biopharmaceutical NMR has been more limited in scope. Chemometrics of 2D-NMR was introduced as a tool for biopharmaceutical higher order structure (HOS) assessment in a 2007 report that compared granulocyte colony-stimulating factor (G-CSF) isolates produced from *Escherichia Coli*. Two statistical approaches were applied to 2D NOESY spectral data using the statistical assessment of peak position and graph invariant theory.¹² The first method performed a direct pairwise comparison on picked-peaks (up to 1000) between G-CSF samples to determine percent comparability. The second method, utilizing

a sequential nearest neighbor model, used the peak coordinates of the most intense peaks (up to 100) as the means of calculating the Euclidean distances. Unfortunately, the two methods gave different similarity metrics, and it was concluded that additional experimental data were needed to ascertain the source of statistical dissimilarity.

Chemometric methods were extended to ^1H , ^{13}C hetero-nuclear single quantum coherence spectroscopy (HSQC)-type experiments for pairwise comparison of a limited number of biopharmaceutical samples spanning a range of molecular weights from 6.5 to 67 kDa. The method, named easy comparability of HOS by NMR (ECHOS-NMR), involved the extraction of a spectral fingerprint region, binning of spectra into 0.05 by 0.5 ppm (^1H and ^{13}C , respectively) buckets, and

Received: January 23, 2020

calculating the Pearson correlation coefficient.¹³ The ECHOS-NMR method was further extended to mAb therapeutics at original digital resolution; thus, no spectral information would be lost.¹⁴ Using this analysis, it was shown that the correlation coefficients determined using 1D isotope-edited and 2D-NMR experiments share a close relationship. While 1D-NMR data can be more rapidly be acquired and analyzed, it was suggested that 2D-NMR spectra be acquired for HOS assessment so that spectral differences could more readily be traced directly back to perturbations in the structure.

The most widely used multivariate statistical method applied to biopharmaceutical 2D-NMR has been principal component analysis (PCA), a technique that greatly reduces the dimensionality of the data and moves the most important variance into the first few synthetic variables, known as principal components (PCs). A number of options have been used for inputting the spectral data into the PCA algorithm; this has included time domain,⁹ peak position in the frequency domain,^{10,15} and the entire spectral region.^{16,17} A small interlaboratory study analyzed filgrastim-based therapeutics, including the originator Neupogen, three foreign-sourced biosimilars, and an in-house uniformly ¹⁵N-labeled system suitability sample (SSS) with the total spectral region as input for PCA.¹⁷ The therapeutic samples and the SSS, which had a small percentage of methionine oxidization, clustered into two distinct groups. However, the clusters also further separated based on the magnetic field strength of the NMR system used for acquisition and the laboratory where the data were acquired, suggesting that inputting the entire spectral region made the analysis especially sensitive to field-dependent effects and subtle differences in experimental setups. A follow-up analysis with a second lot of filgrastim biosimilars using both peak positions and the total spectral region suggested that in the context of an inter-laboratory study with data collected at multiple sites and at multiple magnetic field strengths, the use of peak position provides a more robust input of spectral data for statistical analysis of HOS fingerprints of biologics.¹⁸

Another study, in which acquisition parameters were carefully controlled and spectra collected on a single NMR instrument, reported the exquisite sensitivity of PCA using the full matrix of the spectral fingerprint region in detecting HOS variation between mAb isoforms.¹⁹ In this study, various glycan-remodeled isoforms of the NIST monoclonal antibody (NISTmAb), an IgG1 κ monoclonal antibody developed as a reference material, were prepared enzymatically and compared by spectral overlay, Pearson correlation, and PCA. While no distinctions from visual or pairwise analyses were observed between ¹H,¹³C gradient selected (g)HSQC spectra of the exogalactosylated (ExoGal) and native NISTmAb isoforms, PCA afforded highly sensitive discrimination of the structural isoforms. ExoGal–NISTmAb was further mixed with native NISTmAb from 0 to 100%, and the limit of detection of HOS variation by PCA was determined to be 7.5% relative to the ExoGal–NISTmAb content. In this application, PCA allowed the attribution of small variations in signal intensity to differences in the HOS of the mAb isoforms.

In a seminal biosimilarity study, Japelj *et al.* applied a variety of metrics to 2D-NMR spectra of biologics with the goal of the development of biosimilarity scores for comparative assessment of the small protein filgrastim and the monoclonal antibody rituximab.²⁰ For the filgrastim samples, batches were used from the United States and from the European Union at two different formulations of pH 4.0 and pH 4.4. In addition,

one lot was placed in a deviant formulation of pH 3.0. These metrics, using peak positions as an input, included the *t*-test analogue, PCA, correlation method, distance metrics, hierarchical cluster analysis, tolerance interval approach, and image-difference analysis. The least sensitive metric was determined to be the correlation method, which was determined using chemical shift values. The raw r^2 values decreased only slightly when the comparing the pH 4.4 and pH 3.0 formulations. In the approach using the *t*-test analogue, the locations were derived from the ¹H,¹⁵N cross peaks and the peak widths used as the peak variation. The subsequent results confirmed subtle HOS changes, especially for the batch formulated at pH 3.0. For PCA, both pH 4.0 and pH 4.4 formulations were successfully identified as highly similar, and the outlier at pH 3.0 was outside of the Hotelling's T2 ellipse at the 95% level. Similar results were attained with the hierarchical cluster analysis. The pH 4.0 and pH 4.4 batches, while clustered into their subgroups, had similar distance metrics, and the pH 3 lot identified as an outlier. In the tolerance interval approach, up to 26% of peaks were outside of the defined tolerance interval when the pH was shifted by 1.0 units. Finally, in the image-difference analysis of rituximab batches at different pH formulations, pairwise scores were generated from direct image comparison 2D ¹H,¹H NOESY spectra. Image-difference analysis afforded sensitivity for pH deviations of 0.4 units.

More recently, 1D- and 2D-NMR spectra of different brands of insulin were analyzed using a head-to-head comparison between PCA, sequential nearest neighbor graph invariant (SNN-GI), and 3-way Tucker3 chemometric methods and subsequently quantified the clustering by the Mahalanobis distance.^{21,22} The SNN-GI failed to effectively differentiate the two brands of insulin samples, while the Tucker3 and PCA afforded apparent robust differentiation. While multiway analysis of NMR data has been applied to other fields such as metabolomics and complex mixtures⁴ and has been utilized extensively in spectral reconstruction,^{23,24} this study represented the first application of multiway analysis to classification of biologics. Although Tucker3 did indeed afford discrimination by the two brands of insulin, as measured by the Mahalanobis distance metric, more studies are needed to determine its applicability to higher molecular weight biologics. Each component score of Tucker3 only takes into account one cross peak at a time, and this may be problematic for higher molecular weight biologics or for discriminating between more intricate changes to HOS.

In an effort to benchmark and harmonize the 2D-NMR method for biopharmaceutical applications, a large interlaboratory global study was conducted using 2D-NMR with 26 laboratories from 9 countries, involving pharmaceutical companies, regulatory agencies, government, academia, and one instrument vendor.²⁵ Using a Fab domain derived from the NISTmAb primary sample (PS# 8670)^{26,27} and a uniformly-labeled(U)-¹⁵N,20%-labeled-¹³C-labeled SSS, a total of 451 two-dimensional ¹H,¹⁵N amide, and ¹H,¹³C methyl fingerprints were recorded on 39 different spectrometers, ranging from moderate field of 500 MHz to ultra-high field of 900 MHz, and equipped with conventional and highly sensitive cold probes. The study was designed to measure the ¹H,¹⁵N gHSQC spectrum, which is the "gold standard" for a structural fingerprint of protein folding, for comparability to previous studies. An array of ¹H,¹³C spectral maps were then acquired with both uniform (US) and nonuniform sampling

Table 1. Summary of Required and Optional 2D ^1H , ^{13}C NMR Experiments^a

experiment code	spectra ($N = 375$)	type of experiment	sample	sampling type	comments
Required ^1H , ^{13}C Correlated Experiments					
D2A	39	gHSQC ^b	SSS ^c	US ^d	field independent acquisition: 128 total points in t_1
D2B	32	gHSQC	SSS	NUS ^e	50% NUS of D2A
D2C	41	gHSQC	SSS	US	field dependent acquisition: 25 ms in t_1
D2D	31	gHSQC	SSS	NUS	50% NUS of D2C
D2E	26	gHSQC	SSS	NUS	twice the scans per increment, 50% NUS of D2C
D3A	47	gHSQC	NIST-Fab	US	field dependent acquisition: 25 ms in t_1
D3B	36	gHSQC	NIST-Fab	NUS	50% NUS of D3A
Optional ^1H , ^{13}C Correlated Experiments					
E1	7	gHSQC	NIST-Fab	Either	one parameter change from required experiments
E1A	45	gHSQC	either	NUS	customized sampling schedule
E1B	48	gHSQC	either	either	different temperatures: 15, 25, 45, or 50 °C
E1C	23	sfHMQC ^f	either	either	sfHMQC pulse sequence

^aThis chart was adapted with permission from ref 25, Taylor & Francis Ltd., 2018 (www.tandfonline.com). ^bgHSQC = gradient selected heteronuclear single quantum coherence spectroscopy. ^cSSS = system suitability sample. ^dUS = uniform sampling. ^eNUS = nonuniform sampling. ^fsfHMQC = selective optimized flip angle short transient (SOFAST) heteronuclear multiple quantum coherence spectroscopy (HMQC).

(NUS), different pulse sequences, and at a variety of different temperatures. The spectral maps from all instruments were analyzed using precision metrics such as combined chemical shift deviation (CCSD) and similarity metrics through PCA. Both ^1H , ^{15}N and ^1H , ^{13}C CCSD confirmed a peak position precision of approximately 4 ppb. PCA, conducted on the ^1H , ^{13}C weighted peak positions, afforded rigorous discrimination between the SSS and the NIST-Fab at all temperatures. Most importantly, the 2D-method using weighted peak positions was shown to be both rigorous and reliable, in that the result was independent of field and acquisition strategy.

Despite the advances in the statistics for NMR, there remain open questions regarding the best practices for chemometric analysis of 2D-NMR data acquired for the assessment of biopharmaceutical samples, including how spectral data should be inputted for analysis using any given algorithm. Here, we look at the different ways for spectral data to be pretreated prior to pairwise and multivariate algorithms using two case studies: (1) the multinational interlaboratory NMR study²⁵ and (2) a mixture of NISTmAb glycan-remodeled isoforms. Based on the results, we extrapolate possible best practices for chemometric treatment of NMR data within a biopharmaceutical context.

2. METHODS

2.1. Case Study #1: Multinational Interlaboratory 2D-NMR Study.

The multinational interlaboratory NMR study²⁵ was designed for testing the 2D-method using the ^1H , ^{13}C methyl spectral maps. A brief summary of experiments is given in Table 1. In general, standard ^1H , ^{13}C gHSQC experiments were required to be collected with both US and NUS and in both a field-dependent and independent manner (Table 1, D-type experiment). In addition, each collaborating partner could acquire experiments according to their own laboratory practices (Table 1, E1-type experiments). These experiments included different temperatures, custom sampling schedules, or pulse sequences. No attempt was made to control the absolute signal intensity in any of the experimental designs. Each laboratory was given a unique 4-digit identifier followed by a spectrum number. The experimental code was then appended as a prefix to yield a 10-character spectral identifier. For example, spectrum D2C-7425-012 was performed with D2C experimental parameters by laboratory 7425. The -012 was

the 12th experiment performed by laboratory 7425. Full study and experimental details are given in ref 25.

2.2. Case Study #2: NISTmAb Isoform Blended NMR Data.

The sample series was recreated from ref 19. Briefly, the intact NISTmAb PS #8670 was treated with $\beta(1-4)$ -galactosidase to afford a partially ExoGal intact NISTmAb. The ExoGal-NISTmAb was then blended in various percentages (0, 5, 10, 17.5, 25, 50, 100%) of the native NISTmAb. The nature of the isoforms was confirmed by intact mass spectral analysis in the previous report.¹⁹ The samples were doped with sodium 3-(trimethylsilyl)propane-1-sulfonate- d_6 (DSS- d_6) as a chemical shift reference. The 2D ^1H , ^{13}C spectral maps were acquired with D2B experimental parameters²⁵ at 900 MHz and 50 °C. For statistical purposes, five spectra were collected for each sample, with autosimming performed in-between each experiment. All spectra were processed with NMRPipe²⁸ and visualized with NMRfAM-Sparky.²⁹

2.3. NISTmAb NMR Web Portal: Study Data and Scripts.

NISTmAb-related 2D-NMR spectra for both case studies, including all NMRPipe processing scripts, can be found at <https://www.ibbr.umd.edu/groups/nistmab-nmr>.²⁵ A README file contains instructions to successfully implement these scripts.

3. RESULTS AND DISCUSSION

3.1. Case Study #1: Chemometric Analyses of 2D-NMR Spectra from the Multinational Interlaboratory NMR Study.

3.1.1. Statistical Analyses of Peak Position.

The frequency position of a resonance is an intrinsic NMR parameter of a properly folded protein in a given chemical environment. Much ink has been spilled in attempts to interpret or predict structural details that cause a given atom to resonate at a particular frequency.³⁰ This effort has had some success, as there are a number of reports describing the prediction of secondary structure from a protein sequence and an unassigned peak table.³¹ However, by and large, greater success in utilization of chemical shift data has been achieved if a PDB structure is available.^{32–35}

Despite the complex relationship between structure and chemical shift, this NMR parameter is very robust combined metric of structural and chemical environments and is invariant with respect to acquisition strategy or field strength.²⁵ Indeed,

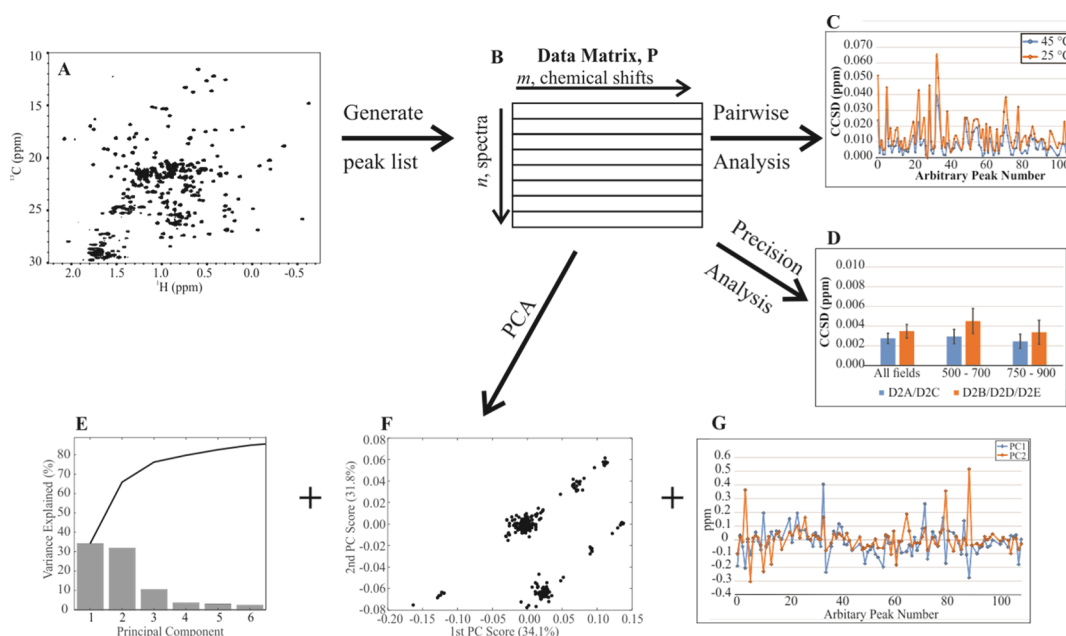


Figure 1. Peak analysis scheme. (A) ^1H , ^{13}C methyl fingerprint from which the peak list is generated. (B) Chemical shift matrix P with n spectra by m chemical shifts. (C) Pairwise CCSD analyses from E1B-6324-014 recorded at 45 °C (blue) and E1B-6324-015 recorded at 25 °C (orange), both referenced against D2A/D2C average peak list. (D) Average CCSD. Subsequent PCA analysis afforded the (E) scree plot, (F) score plot, and (G) peak loading plot.

the chemical shift is not only repeatable in the same laboratory with multiple operators, but the multinational NMR interlaboratory study established that peak position is reproducible to within 4 ppb for controlled experimental parameters. For uncontrolled parameters, the precision only falls to 6 ppb. If sample conditions are carefully matched (e.g., concentration, salinity, pH), then any peak list represents a spectral fingerprint of the drug substance and any change can be attributed to a perturbation in the HOS. If resonance assignments are known, then these observed perturbations can be mapped directly onto the protein structure, and the spectral map becomes a true “structural fingerprint”. However, resonance assignments, though helpful, are not required because an arbitrary peak list table can be defined and used to define the HOS of a biopharmaceutical.^{18,25} In Section 3.1, we provide current best practices for pairwise and multivariate analysis of peak list tables derived from 2D-NMR spectra (Figure 1).

3.1.2. Generation of Peak List. Defining a peak list is the fundamental component of any type of analyses involving chemical shifts. Any peak list needs to be properly referenced against the established NMR chemical shift standard of DSS.³⁶ In general, an average S/N threshold needs to be defined for the peaks. This value can be defined based on the need of a given application, although in practice, a minimum of 10:1 is commonly used.^{25,37} As with most analytical techniques, the accepted limit of detection (LOD) is a S/N of 3:1,³⁷ and metrics correlating multiple NMR spectra are typically not as reliable below the S/N value of 10:1.¹⁴ Second, the peaks need to be resolved; this can include high intensity peaks within a very crowded region, although care must be taken that a given peak could, in reality, be more than one overlapped peak. Peak-picking was, however, used reliably within a heavily crowded ^1H , ^{13}C methyl region for the multinational interlaboratory study.²⁵ In practice, there are many NMR software packages such as NMRFAM-Sparky,²⁹ NMRPipe,²⁸ NMRViewJ,³⁸ and

NMR vendor-specific software that can adequately define the peak list, although analyst intervention is necessary to ensure proper curation of the list (Figure 1A). If resonance assignments are available, the chemical shifts can be directly mapped onto the amino acid sequence. Otherwise, the analyses can continue with an arbitrarily defined peak list. For the interlaboratory study, 22 datasets did not meet the S/N threshold requirement of 10:1 or otherwise had some other known experimental error; only 353 datasets were therefore used for this type of analyses.

3.1.3. Analysis of Peak Precision through Root Mean Square Analysis and CCSD. One of the conventional methods to analyze the precision of the peak positions between multiple 2D spectra is using root mean square deviation (rmsd),^{17,39} which is defined as

$$\text{rmsd} = \sqrt{\frac{1}{n} \sum_i^n \delta_i^2} \quad (1)$$

where n is the number of spectra and δ_i is the chemical shifts, separately, of ^1H , ^{13}C , or ^{15}N in ppm. The rmsd of each peak can then be plotted for the entire peak list for each nuclei of interest. If the rmsd plots are to be compared for the different nuclei, then a frequency weighting factor needs, α_i , to be applied

$$\text{rmsd}_{\text{weighted}} = \sqrt{\frac{1}{n} \sum_i^n (\alpha_i \delta_i)^2} \quad (2)$$

where α_i is 1.0 for ^1H , 0.251 for ^{13}C , and 0.10 for ^{15}N , according to the relative magnetogyric ratios of these atoms.

Alternatively, and more commonly employed, eq 2 is transformed into the weighted average of the ^1H and the heteronucleus (e.g., ^{13}C or ^{15}N) chemical shifts for the same cross peak between two spectra. This type of weighted average is known as CCSD

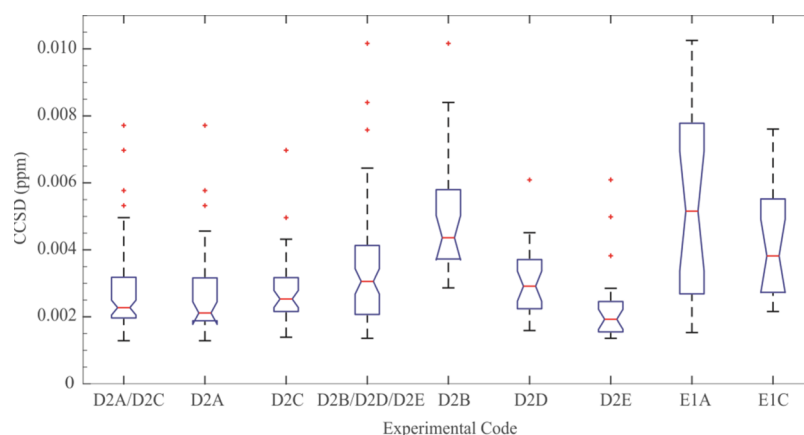


Figure 2. Box plot of CCSD analysis of multinational interlaboratory NMR study. Error bars, often referred to a “whiskers,” represent the 1.5 times the upper and lower interquartile range. The median line is shown as a red line. Data outliers are shown as individual red points. See main text for a complete description of a box plot. A summary of experimental codes is given in Table 1.

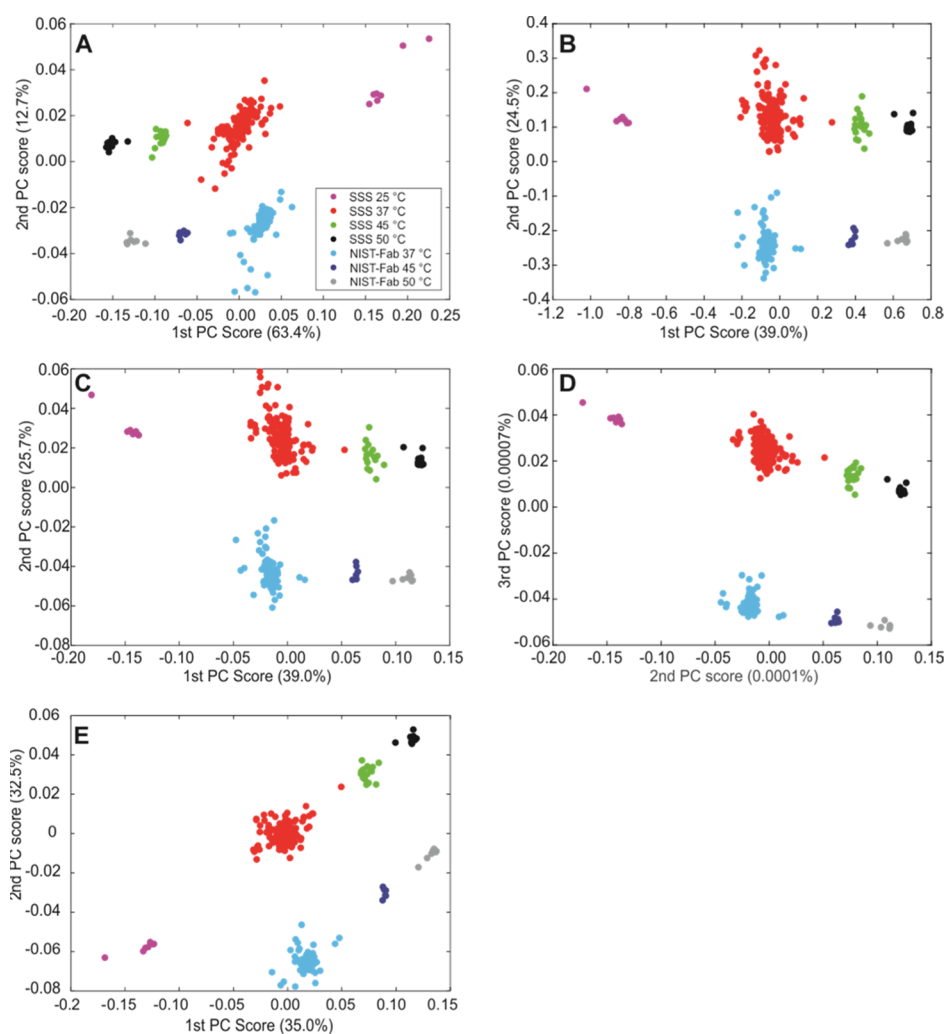


Figure 3. PCA plots of the interlaboratory multinational NMR data package, using various normalization routines for analysis. (A) ^1H peak tables, centered; (B) ^{13}C peak tables, centered; (C) weighted $^1\text{H},^{13}\text{C}$ peak tables, centered. For panels (A–C), the centering was accomplished by subtracting the column means before performing PCA. (D) Weighted $^1\text{H},^{13}\text{C}$ peak tables, not centered; (E) weighted peak tables normalized against D2A/D2C reference datasets by subtracting the average D2A/D2C reference chemical shift values from each spectrum.

$$\text{CCSD} = \sqrt{\frac{1}{2}[(\delta_{\text{H}} - \delta_{\text{H,ref}})^2 + (\alpha_i \delta_i - \alpha_i \delta_{i,\text{ref}})^2]} \quad (3)$$

where δ_{H} and δ_i are, respectively, the ^1H and ^{13}C or ^{15}N chemical shifts of a subject cross peak; $\delta_{\text{H,ref}}$ and $\delta_{i,\text{ref}}$ are, respectively, the ^1H and ^{13}C or ^{15}N reference chemical shifts for the same cross peak. Pairwise plots can be generated to

visualize the CCSD across the entire peak list between any two spectra from the reference library (Figure 1C). For a true precision analysis for multiple spectra collected on a drug substance under highly similar sample and experimental conditions, the average CCSD can be plotted (Figure 1D). Error bars are reported using the standard error of the mean (SEM), typically with 95% confidence intervals

$$\text{SEM} = \mu \pm 1.96 \times \frac{\sigma}{\sqrt{n}} \quad (4)$$

where μ is the average CCSD and σ is the sample standard deviation. However, a standard bar plot may hide the true deviation of the data, and outliers may be missed, especially if the sample size is large.

Another means to visualize the precision of the measurement is via a box plot (Figure 2). The median of the data is plotted followed by a box that represents the 75th and 25th percentiles. If the median line is not in the center of the box, then it can easily be visualized that the data is skewed. The error bars, often referred to a “whiskers,” represent the 1.5 times the upper and lower interquartile range. Any outliers outside of this range are then plotted as individual data points.

3.1.4. Analysis of Multiple Peak Lists Using PCA. A data matrix, P , is established by listing all spectra in rows (n) and each table of chemical shifts (m). Many different preparations have been done to prepare the peak tables for the matrix. These include simply subtracting the ^1H and X (^{13}C or ^{15}N) frequency-weighted chemical shifts from the average values before concatenation.¹⁰ To date, biopharmaceutical NMR applications have used single concatenation of unweighted chemical shifts²⁰ or have used weighted chemical shifts according to eq 5.^{18,25}

$$\delta_{\text{weighted}} = \sqrt{\frac{1}{2}[(\delta_{\text{H}})^2 + (\alpha_i \delta_i)^2]} \quad (5)$$

Alternative treatments of peak tables prior to PCA are explored more fully, below.

After pretreatment of peak tables, a matrix P of n spectra by m chemical shifts is generated (Figure 1B). PCA is then performed (Figure 1E–G), most often with singular value decomposition (SVD), as defined by

$$P = U\Sigma V^T \quad (6)$$

where U is the left singular vector and represents a matrix defining the PC scores. The singular values are defined in the diagonal matrix Σ , represent the eigenvalues ($\sigma_1, \sigma_2, \sigma_3, \dots, \sigma_n$), and are organized in descending magnitude. The matrix V is the right singular vectors and represents the eigenvectors of P . The PC scores, often multiplied by their respective singular values to give a visual indication of their importance, are plotted (Figure 1F). Typically, the first few PCs contain the greatest information of interest, and later PCs contain only random experimental noise. To qualitatively determine how many PCs to retain, a scree plot graphs the degree of variance explained by each PC (Figure 1E). PCs at and below the “elbow” in the curve are typically retained for more detailed analyses, although knowledge of the nature of the sample type is also critical for this decision, as will be seen below. Finally, performing PCA on spectral data affords peak loading plots, directly derived from the plotting of V (Figure 1G), and the influence of each peak position in each PC can be quickly visualized. These plots allow the identification of peak positions that account for the observed variance in the data.

The most important step in this method is the decision about preprocessing of the peak list data and whether to use any normalization prior to PCA. For most applications of PCA on other types of analytical data, the data are centered by subtracting the mean of each column.⁴⁰ For NMR spectral data, for which each cross peak is directly traceable to the frequency position, centering may not intuitively be the optimal option because the magnitude in each PC may putatively be a chemical shift change indicative of a structural perturbation. As such, a series of data inputs were prepared using a few representative normalization routines: ^1H chemical shifts; ^{13}C chemical shifts; and $^1\text{H}, ^{13}\text{C}$ weighted chemical shifts (Figure 3). As can be seen, all chemical shift data inputs afforded qualitatively similar plots, regardless of data pretreatment. However, inputting the weighted combined $^1\text{H}, ^{13}\text{C}$ chemical shifts as-is without centering affords the visually tightest clusters (Figure 3D). For this data input, the first PC approximates the average chemical shift for each peak and therefore accounts for 99.9999% of the data. This apparent anomaly illustrates the importance of understanding the nature of the data input and reduces the reliability of the scree plot for use with 2D-NMR data inputs. For panel D, the important chemical shift changes are in the ppb range, whereas the average chemical shift is in the ppm range. The important clustering information therefore is pushed out to PC2 and PC3.

While all plots given in Figure 3 clearly separate out into the expected seven clusters, a biopharmaceutical laboratory typically establishes an internal reference standard in the development of each biologic. As such, the 2D-NMR method should adhere to this standard practice and normalize all data to the product-specific reference standard. For the interlaboratory international NMR data package, to simulate this situation, the D2A and D2C datasets were used to define the average reference chemical shifts for each peak, and each peak table was subtracted from this reference (Figure 3E).

While chemical shift data are highly precise and have proven to be a very rigorous HOS parameter for biopharmaceutical applications, this NMR parameter may not be sensitive to all aspects of HOS. For example, some changes to HOS may result in appearance of new peaks⁴¹ that are not taken into account by a simple peak table comparison. While methods of comparing peak tables of varying sizes can be envisioned, these have yet to be applied to biopharmaceutical applications. Furthermore, a shift in the conformational ensemble of a drug substance might simply result in changes only in peak linewidth and/or intensity.¹⁹ Such changes in the cross peak signatures could indicate the possible formation of soluble aggregates, an important quality attribute that chemical shift information by itself may miss. To ameliorate these concerns, peak tables containing more peak information such as line widths or peak intensity could be added into the data matrix. While this has been proposed in several reports in other NMR fields,^{42,43} to date this has not been performed in a biopharmaceutical application. For biopharmaceuticals, measurement of peak line width is normally impractical due to the higher molecular weight of these drugs that limits peak resolution. Peak intensity, however, can easily be extracted from spectra of the drug substances.

To address the impact of the use of peak intensity data in the analysis of the interlaboratory study, all cross peaks were normalized to the most intense peak, which was then set to a value of 100. The data matrix was then prepared with only the

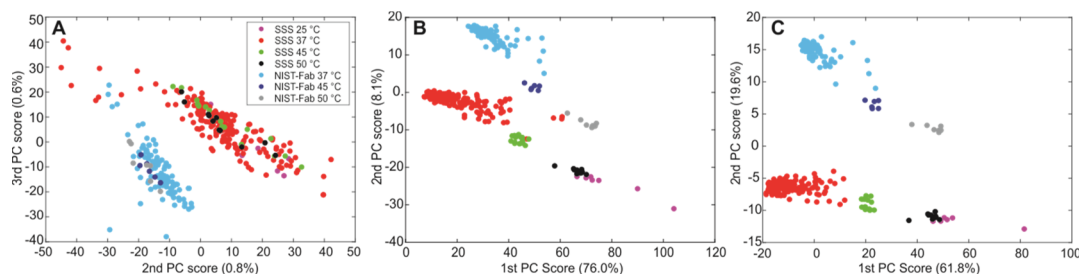


Figure 4. PCA plots of peaks tables with peak intensity. (A) Raw peak intensity at each peak position, centered; (B) Malmström distance, centered; (C) Malmström distance with EIA custom NUS datasets and EIC sfHMQC datasets removed, centered. The centering was performed in the manner described in Figure 3. The corresponding uncentered PCA plots looked very similar to those in this figure (data not show).

intensity value at each peak position. After PCA, only two loose clusters of the SSS and the NIST-Fab data, rather than the expected seven clusters, were observed (Figure 4A). This result is unsurprising because peak intensity is a parameter that is difficult to control, and no effort was made to control it for this study.

A recent study by Malmström and co-workers made an attempt to combine chemical shift and intensity information for each peak by dividing each peak parameter by its corresponding variance.⁴⁴ The following equation computes the overall distance, D_{sum} , of a given spectrum from a reference dataset

$$D_{\text{sum}} = \sum_{i=1}^n \sqrt{\frac{((\delta_{\text{H},i} - \delta_{\text{H,ref}})^2)}{\text{var}({}^1\text{H})} + \frac{((\delta_{\text{C},i} - \delta_{\text{C,ref}})^2)}{\text{var}({}^{13}\text{C})} + \frac{((I_{\text{O},i} - I_{\text{ref}})^2)}{\text{var}(\hat{I})}} \quad (7)$$

where $\delta_{\text{H},i}$, $\delta_{\text{C},i}$ and $I_{\text{O},i}$ are, respectively, the ${}^1\text{H}$ and ${}^{13}\text{C}$ chemical shifts and the intensity value of a subject cross peak in the i th spectrum; $\delta_{\text{H,ref}}$, $\delta_{\text{C,ref}}$ and I_{ref} are, respectively, the ${}^1\text{H}$ and ${}^{13}\text{C}$ reference chemical shifts for the same cross peaks and the intensity value for the reference cross peak. The denominator of each term, $\text{var}({}^1\text{H})$, $\text{var}({}^{13}\text{C})$, and $\text{var}(\hat{I})$, corresponds to the respective variance. The resulting Malmström distance can then be used for pairwise analysis of a few spectra against a reference.

A simple reformulation of the Malmström equation removes the sum from the equation, affording a resonance distance, D_{res} , for each peak within a spectrum from its corresponding average reference peak from the D2A/D2C datasets.

$$D_{\text{res}} = \sqrt{\frac{((\delta_{\text{H}} - \delta_{\text{H,ref}})^2)}{\text{var}({}^1\text{H})} + \frac{((\delta_{\text{C}} - \delta_{\text{C,ref}})^2)}{\text{var}({}^{13}\text{C})} + \frac{((I_{\text{O}} - I_{\text{ref}})^2)}{\text{var}(\hat{I})}} \quad (8)$$

All variables are defined as in eq 7. For the analyses herein, the variance was defined from the reference D2A/D2C datasets. The distance, D_{res} , is then computed for all resonances within a peak list, and a matrix can then be formulated in a manner similar to the matrix for weighted chemical shifts (Figure 1).

After performing PCA, most of the expected clusters were observed (Figure 4B,C). The exception is the spectra collected at 25 °C. Because of the referencing of the peak position to spectra collected to 37 °C, the squaring of the spectral values for the 25 °C spectra had the effect of shifting these points by the 50 °C cluster, such that neither cluster can be defined well. Further, removing spectra that have intrinsically different intensity values due to nonstandard acquisition strategies (e.g., EIA spectra with custom NUS schedules and EIC spectra) did not improve the separation of these two clusters. Overall, this treatment of the data provided the best result to date but still

yields inferior clustering when compared to the use of only chemical shifts.

3.1.5. Chemometric Assessment of Manually Defined Clusters. From visual inspection of Figures 3 and 4, the clustering in Figure 3 appears to be useable for evaluation of spectra, although the scatter of the points appears to be slightly greater for panels A through C. Conversely in Figure 4B,C, the cluster separation appears visually reduced, and the overlap of the SSS 45 and 50 °C clusters suggests that the data input using Malmström distance may be suboptimal for chemometric assessment. In practice for biologics applications, a metric is needed to evaluate cluster compactness. A few representative examples of commonly used metrics include the Euclidean distance from a given point in a cluster to its centroid, Davies–Bouldin index,⁴⁵ silhouette values,⁴⁶ the Dunn index.^{47,48} While it is beyond the scope of this study to evaluate all such metrics, the varied data inputs from Figures 3 and 4 represent a challenge because each input represents different distance units, whether it be chemical shifts alone, weighted chemical shifts, or intensity; thus, a metric needs to be chosen that addresses and mitigates the problem of the different data inputs.

Despite the challenges in using some distance-based metrics, the Dunn index provides a reliable means of cluster assessment.^{47,48} The metric was motivated, in large part, to the ambiguity in defining the size of a cluster. The size could be defined as a radius or the length of a perimeter; it could be the distance between two points inside the cluster or some average distance. The Dunn index seeks to eliminate this ambiguity and gives large values to those clusters with small variance within a cluster while being well separated from other clusters. The metric rewards a clustering where different clusters have different statistics. One way to think of this (without defining it precisely) is the higher the Dunn index the more “compact” the clusters are. The compactness Δ_i of a cluster C_i is given by

$$\Delta_i = \frac{1}{|C_i| - 1} \sum_{x \in C_i} d(x, a_i) \quad (9)$$

where x represents any point and a_i represents the centroid of cluster C_i . Let $\delta(C_i, C_j)$ be the intercluster distance defined as

$$\delta(C_i, C_j) = d(a_i, a_j) \quad (10)$$

where a_j is the centroid for cluster C_j . The Dunn index DI is then given by

$$DI = \frac{\min_{1 \leq i \leq j \leq m} \delta(C_i, C_j)}{\min_{1 \leq k \leq m} \Delta_k} \quad (11)$$

The Dunn index affords a clear distinction between the data inputs with and without peak intensity (Figure 5). As expected,

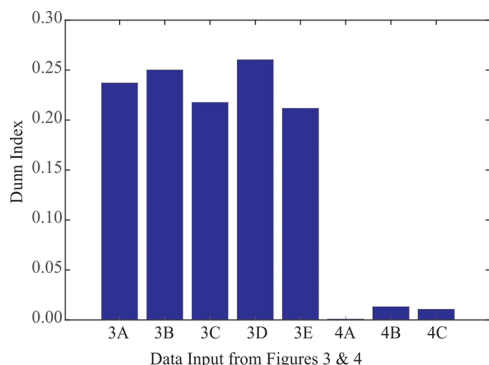


Figure 5. Dunn index of data inputs from Figures 3 and 4. The x -axis indicates the figure and panel from which the data input was derived.

inclusion of peak intensity information is far inferior to chemical shift alone, for which all bars are of the same magnitude. The Dunn index therefore provides a quick qualitative metric on the clustering assessment. However, it is imperfect, as data input 3A appears to be slightly better than data input 3E, when visually 3E looks better than 3A (Figure 5). Furthermore, the Malmström distance (Figure 5, bars 4B,C) is superior to intensity information alone.

Another metric used to validate clusters is known as the silhouette value, which is the measure of the cohesion of a given data point to its own cluster relative to a neighboring cluster.⁴⁶ For a given data point $x(i)$ in cluster C_i

$$x(i) = \frac{1}{|C_i| - 1} \sum_{j \in C_i, i \neq j} d(i, j) \quad (12)$$

The smaller that the value of $x(i)$ determines how well the assignment is to a given cluster. Next, the dissimilarity of point i to another cluster is defined as

$$y(i) = \min_{k \neq i} \frac{1}{|C_k|} \sum_{j \in C_k} d(i, j) \quad (13)$$

The term $y(i)$ is the distance of point i to all other points not in C_i . The neighboring cluster has the smallest mean dissimilarity. Each data point is given a silhouette value $s(i)$, which is defined as

$$s(i) = \frac{y(i) - x(i)}{\max\{x(i), y(i)\}}, \quad \text{if } |C_i| > 1 \quad (14)$$

This has the effect of normalizing the $s(i)$, such that

$$-1 \leq s(i) \leq 1 \quad (15)$$

Values of $s(i)$ that approach 1 suggest that it has likely been given the correct cluster assignment. Values below 0 indicate an incorrect assignment, whereas values near 0 represent an ambiguous assignment.

Representative silhouette plots from selected data inputs (from Figures 3E and 4C) show that most of the spectra are correctly classified because the $s(i)$ values are greater than 0.6

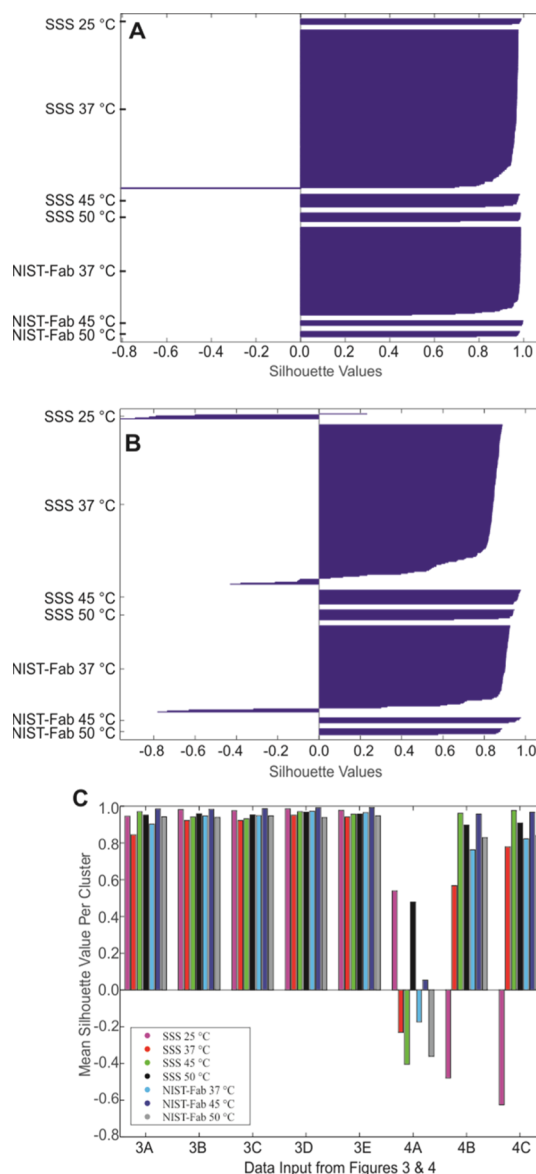


Figure 6. Assessment of clusters using silhouette values. Two representative examples of silhouette plots are provided in (A) weighted normalized peaks from Figure 3E; and (B) Malmström distance from Figure 4C. For both of these plots, each spectrum is represented as an individual bar. In panel A, the sole outlier is discussed in detail in ref 25. (C) Mean silhouette values per cluster per data input from Figures 3 and 4.

(Figure 6A,B). For panel A, only 1 clear spectral outlier is identified, which was due to a temperature mis-setting.²⁵ Panel B shows a greater number of spectra with negative $s(i)$ values, confirming the visual inspection that some of the clusters are not that well defined when the Malmström distance is applied before PCA. Figure 6C gives the mean silhouette value for each manual cluster, allowing a quick assessment of cluster consistency from all data inputs. While this once again confirms that all 5 data inputs with only chemical shift data afford good cluster consistency, it is noted that the silhouette value for the SSS-37 °C cluster for the ¹H chemical shifts is slightly reduced (entry 3A), confirming the visual observation of the slightly greater point spread. For the data inputs with both chemical shifts and peak intensity values,

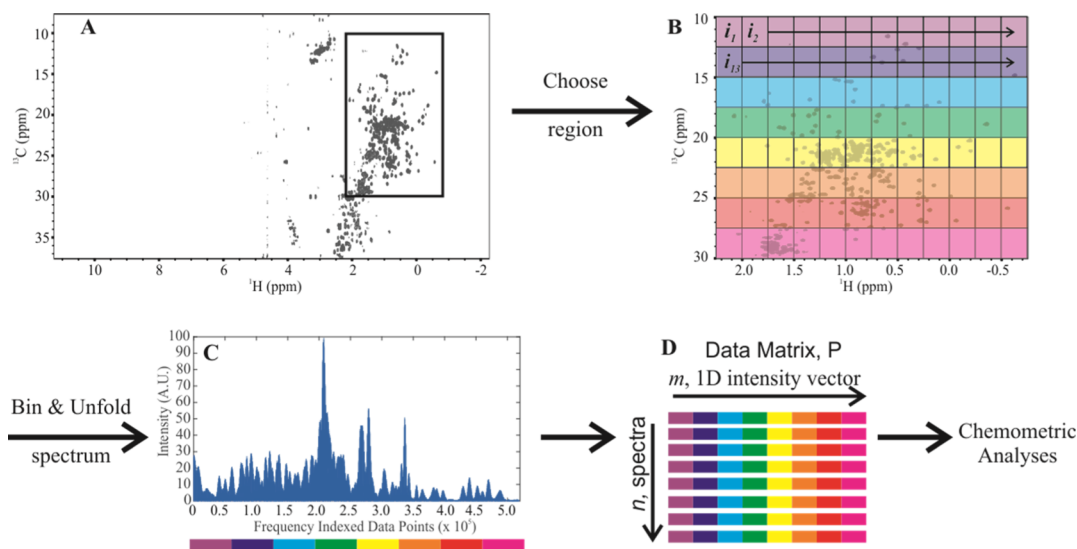


Figure 7. Spectral analysis scheme using total point-by-point matrix as input into chemometric algorithms. (A) Entire ^1H , ^{13}C gHSQC spectrum optimized for the methyl group. The boxed area was the fingerprint region extracted. (B) Spectrum is then binned, typically to the digital resolution, affording hundreds of thousands of points, depending on original processing of the time domain. Using the default processing of the interlaboratory data package, greater than 500,000 points comprise the spectral region. (C) Rows are then unfolded to afford a 1D intensity vector. (D) Data matrix P is formed with n spectra by m intensity vectors.

the negative mean silhouette values for the SSS-25 $^{\circ}\text{C}$ clusters verifies the lack of cluster consistency.

In general, both the Dunn index and silhouette values provide a means to validate which data inputs affords the greatest cluster consistency in the PCA score plots. In the case of the interlaboratory study data, chemical shifts alone provide the best clustering in the analysis of the data.

3.1.6. Alternative Data Input: Analysis of Total Spectral Region. While the development of peak tables can be labor intensive, a spectrum in the frequency domain can be treated as a matrix of frequency-referenced points with intensity values binned to the digital resolution of the spectrum (Figure 7). A desired fingerprint region is often extracted, although the exact chemical shift ranges need to be tailored to the actual spectral fingerprint of a specific biologic. The “gold standard” for assessment of proper protein folding is the ^1H , ^{15}N amide region, which provides a read-out of each ^1H , ^{15}N amide correlation for every nonproline amino acid from the ^1H , ^{15}N spectral maps. However, spectral fingerprinting using ^1H , ^{13}C methyl spectral has become increasingly utilized due to not only the intrinsic higher sensitivity of the ^{13}C nucleus but also the favorable NMR parameters of the methyl moieties from its free rotation around the sp^3 bond⁴⁹ and its relative insensitivity to pH and ionic strength.

Whether a spectral fingerprint is defined from the amide, methyl region, or some other region, the subsequent data handling is the same and is illustrated with spectra from the multinational interlaboratory study (Figure 7). After selection of the desired region, each row or column is extracted and concatenated to form a 1D intensity vector (Figure 7A,B). These vectors will be on the order of several hundred thousand points, depending on the original spectral processing, and each pixel is frequency-encoded with intensity information. For direct comparison, each 1D intensity vector needs to be the same size; interpolation may be needed for vectors of different sizes. The intensities of each spectrum are most commonly normalized to a predetermined value for the most intense pixel in the spectrum. This normalization gives a qualitative

comparison between all spectra, assuming that the same acquisition strategy and magnetic field are used. Such treatment will retain all spectral information, including not only peak position but also linewidth and peak intensity. Applying this approach to the ^1H , ^{13}C spectral maps from the interlaboratory NMR study using the default spectral processing scripts, each spectrum was normalized so that its maximum intensity was set to the arbitrary value of 100. In order to apply PCA directly to the matrix of intensities, data from each spectrum must correspond on a point by point basis. To achieve this for a collection of spectra measured at different field strengths and a variety of acquisition methods, all spectra were interpolated relative to spectrum D2C-8822-010 using bilinear interpolation, affording the exact same size and chemical shift range as D2C-8822-010. The methyl fingerprint region was defined as -0.7 to 2.20 ppm in ^1H and 8.0 – 28.0 ppm in ^{13}C . Extraction of this region afforded 1D intensity vectors with over 500,000 points each (Figure 7C).

Another consideration in data preparation when using the total spectral region is noise treatment. Often, especially for spectra with low amplitude random noise, the noise may be left untouched. Another method involves computing the root mean square noise and setting all intensity values times a predetermined factor below this threshold equal to zero.^{50,51} While several different factors have been used, a good rule of thumb is a factor of less than three because the LOD for NMR is considered to be 3-to-1.³⁷ For situations of spectra with high amplitude noise or deterministic noise from NUS, different noise thresholding may be used, although best practices are not yet established for these situations. For all analyses of the interlaboratory study data, it was determined empirically that noise pretreatment of the data had only a negligible effect, and therefore the noise was left untouched in the following analyses (data not shown).

In general, analyses of spectra as 1D intensity vectors offers a truly unbiased approach with minimal data manipulation prior to chemometric analysis. For the comparison of a few spectra, pairwise analysis can be performed on 1D intensity vectors. For

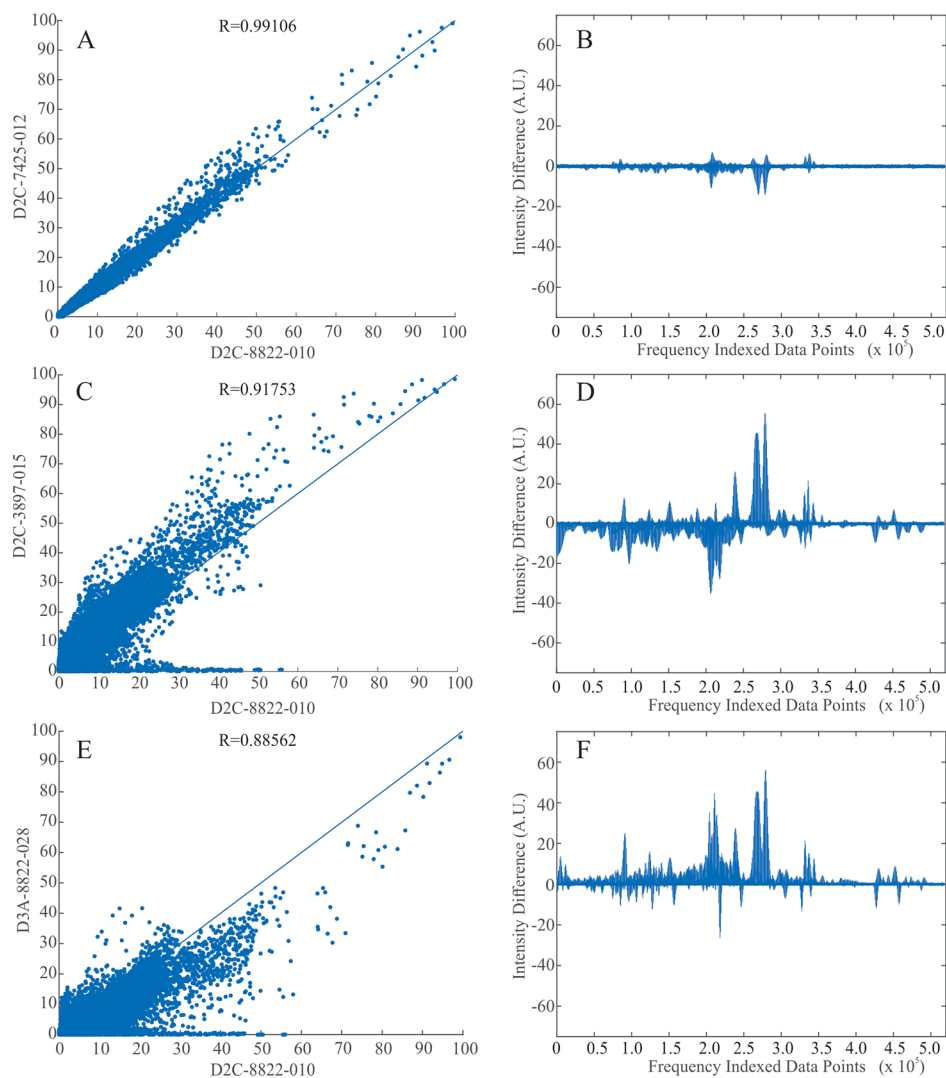


Figure 8. Correlation and intensity difference plots referenced against D2C-8822-010 of the SSS collected at 900 MHz. (A,B) D2C-7425-012 of the SSS collected at 900 MHz; (C,D) D2C-3897-015 of the SSS collected at 500 MHz; (E,F) D3A-8822-028 of the unlabeled NIST-Fab at collected 900 MHz. In panels (A,C,E), the reference line indicates the demarcation of perfect correlation between corresponding points in the two spectra. The Pearson coefficient (R) is listed about each plot.

analysis of a greater number of spectra, the 1D intensity vectors can be organized in an $n \times m$ matrix before applying further chemometrics (Figure 7D).

3.1.7. Analysis of the Total Spectral Region by Pairwise Analysis. For the comparison of two 1D intensity vectors, the Pearson correlation coefficient, R , can be determined.¹⁴ Such a metric can provide a quick qualitative assessment of the similarity of two 2D-NMR fingerprints (Figure 8). The difference in correlation between the two 1D intensity vectors can be computed to more easily evaluate apparent spectral regions that appear to deviate from the reference (panels B, D, F). A comparison of two spectra collected at 900 MHz on the SSS affords a very high R of 0.991. However, this value drops to 0.918 when comparing spectra collected at 500 and 900 MHz, showing a field effect for spectra otherwise acquired with the same experimental parameters. For the SSS and NIST-Fab spectra at 900 MHz, the R value drops to 0.886, which is only slightly lower than the SSS at two different fields. This apparent trend can be confirmed by plotting the R values for all D-type experiments from the interlaboratory study data package, showing the relative insensitivity of the method to

distinguish the SSS spectra from NIST-Fab spectra, even though the primary sequence of the SSS has four extra alanines (Figure 9). At 900 MHz, there is some differentiation between the two samples, but there is none at 500 MHz. This field dependence suggests that the pairwise analyses using the Pearson correlation can only be reliably used for the same acquisition strategy and field strength, and that this approach is not ideal for lower field datasets that may be limited by S/N and/or resolution. In addition, while the determination of Pearson coefficient may have limited applicability for a few spectra, other chemometric approaches are more robust for large numbers of spectra.

3.1.8. Analysis of the Total Spectral Region by PCA. For large datasets with many spectra, PCA offers a powerful unsupervised means to reveal similarities and differences between spectra and relate these to similarities and differences in the samples. As described above, the matrix P is constructed to give n spectra by m number of points per spectra vectors (Figure 7D). PCA offers the advantage of simultaneously analyzing 500,000th dimensional space (the number of points for the methyl region from the interlaboratory NMR study

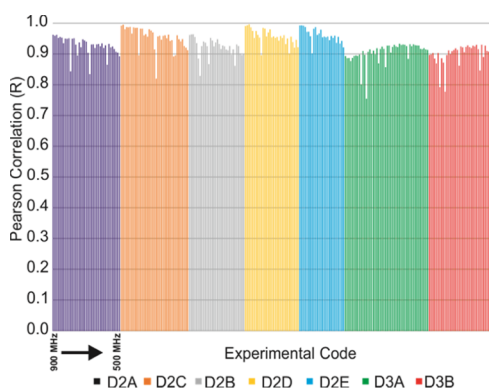


Figure 9. Pairwise analysis using the Pearson correlation coefficient of all required D-type experiments from the international interlaboratory NMR study. All spectra are referenced to spectrum D2C-8822-010 collected at 900 MHz. For each experimental code, the left most R values were of spectra recorded at 900 MHz. The field strength gradually decreases to the right, as labeled for D2A-type spectra.

spectra) and thereby reducing the dimensionality of the data down to a few important independent variables, typically 2–6 PCs (Figure 10). Beyond a critical number of PCs, mostly noise is found. In practice, the number of components required depends on the diversity of sample content. This is due to the fact that each PC is a linear combination of all of the spectra in the series, sorted in order of how much of the data is approximated by a given component. For example, if there were a series of ideal, noise-free spectra of samples containing mixtures of three noninteracting compounds in different ratios, only three components would be needed to describe the series exactly, no matter how many spectra the series contained. In a more realistic version of this example with actual spectral data, components must encode both the variation due to sample and the variation due to measurement. In the example of the study data, there are only two samples, but substantial variation in measurement, including different temperatures and field strengths, so more than two components are needed to describe the data series to within the noise.

The direct matrix PCA examples here calculate components by SVD, which always computes all components, or by NIPALS.⁵² NIPALS has the advantage of being able to select the number of components to calculate, without the need to determine them all, even though most components might consist only of noise. Components are calculated without applying centering (subtraction of the average spectrum). In these cases, the first component approximates the average spectrum.⁵²

The 3D PCA plot of the interlaboratory NMR data affords “fuzzier” clustering than the PCA plots based on peak tables (Figure 10). If the complete data package is used, proper differentiation of the known groupings is obscured, due to the spectral variations associated with the plethora of acquisition methods employed by each group in the study (Figure 10A). Because these experimental variations impact the intensity of each peak, PCA was performed on only the D-type and E1B experiments, for which the acquisition methods were required to be more similar (Figure 10B). In addition, the 15 °C datasets were removed in panel B due to the fewer number of spectral maps recorded at this temperature. By taking these steps, clear separation can be observed between the SSS and the NIST-Fab, and separate clusters based on temperature can be visually discerned, although these are less defined when compared to the analyses using the chemical shifts from the peak tables. Upon closer inspection, the points appear to spread according to spectral resolution, from 500 to 900 MHz at all temperatures (Figure 10B, see label).

One substantial advantage of direct matrix PCA is the ability to visualize PCA eigenvectors (loadings) as spectra (Figure 11). This will highlight which peaks are changing and also show whether the observed variation is due to change in peak position or other peak parameters such as line widths. As shown in Figure 11, many of the signals in the second component consist of a positive center with symmetric negative lobes on either side of the ¹³C dimension. This is characteristic of stationary chemical shifts and varying linewidths, as expected for measurements of the same sample at different field strengths.

PCA of the total spectral region of the interlaboratory NMR data package underscores the lack of robustness of this approach for data analysis when spectral intensity matrices are derived from multiple fields and acquisition methods. While all spectra were normalized to the most intense peak in the spectrum, this peak may be different in each spectrum depending on the pulse sequence used (gHSQC vs sfHMQC) or sampling method employed (US vs NUS). Furthermore, the intrinsic difference in resolution and relaxation effects that depend on the magnetic field strength used additionally compromises the application of PCA in this context. Attempts to mitigate these effects by applying line-broadening factors during processing offered only minimal improvement (data not shown). While not interpretable in the context of the interlaboratory study design, it is well known that the peak shape and intensity contains a wealth of information regarding conformational dynamics and quaternary interactions. In the next section, a case study was designed to show the power of

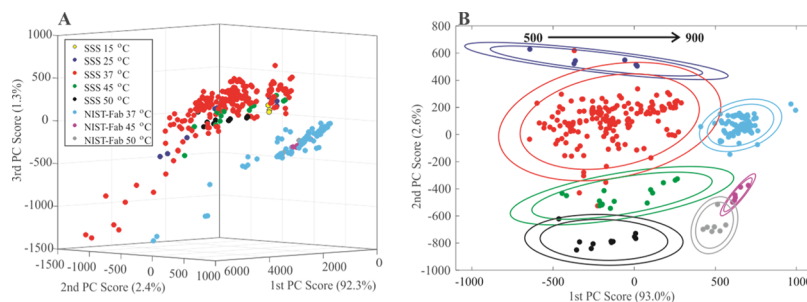


Figure 10. PCA plots of the total point-by-point fingerprint region. (A) All spectra from the interlaboratory study; (B) all D-type and E1B-type experiments. In panel (B), the field dependence in PCA space from 500 to 900 MHz is labeled.

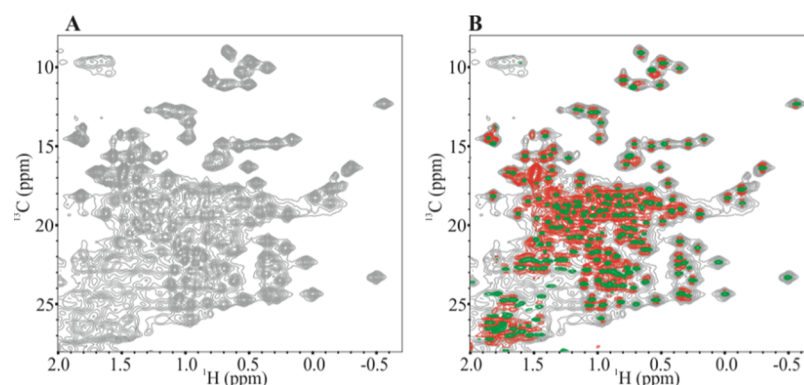


Figure 11. Spectral loading plots from PCA of D-type and E1B experiments. (A) PC1; (B) PC2 on PC1. Positive contours are in green and negative contours are in red.

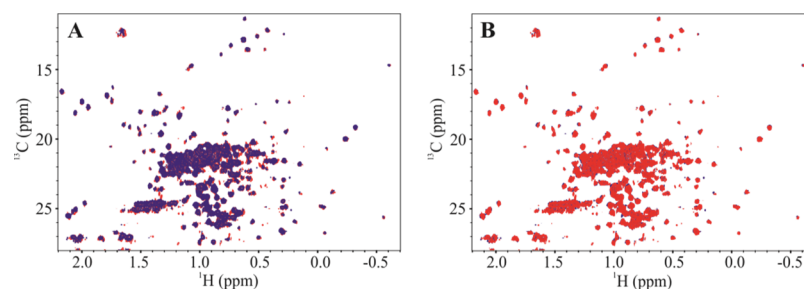


Figure 12. Visual comparison of spectral overlay of NISTmAb in blue and ExoGal–NISTmAb in red. (A) NISTmAb on ExoGal; (B) ExoGal on NISTmAb.

applying PCA analysis to the total spectral matrix for HOS assessment and confident identification of HOS variation as revealed through differences in peak shape and intensity.

3.2. Case Study #2: Chemometric Analyses of 2D-NMR Spectra of NISTmAb Glycan-Remodeled Isoforms.

A second spectral data series was prepared to illustrate the strengths and weaknesses of peak table analysis *versus* the total spectral matrix in the use of 2D-NMR data for HOS assessment. The previous report by Arbogast *et al.*¹⁹ illustrated the great sensitivity of analyzing the total spectral matrix for differentiating glycan remodeled isoforms of NISTmAb. However, it was reported that visual inspection ^1H , ^{13}C spectra of the NISTmAb *versus* ExoGal–NISTmAb isoform showed high spectral identity, raising the question if a rigorous peak table analysis would similarly differentiate between the two types of samples. To test this possibility, the sample series was recreated. The ExoGal–NISTmAb was blended in various percentages (0, 5, 10, 17.5, 25, 50, 100%) of the native NISTmAb, and five 2D ^1H , ^{13}C spectral maps of each sample blend were collected.

3.2.1. Analysis of Peak Positions of Case Study #2. Visual inspection of the ^1H , ^{13}C spectral maps of the NISTmAb and ExoGal–NISTmAb afforded the expected highly similar overlay, with only slight differences apparent after close inspection (Figure 12). Development of a peak list for an intact mAb is a greater challenge than for the Fab domain alone because the linewidth is inherently broader due to the greater molecular weight and slower rotation correlation time. This problem is slightly ameliorated by raising the temperature to 50 °C. Further, to minimize the amount of overall experimental time and minimize degradation from the high temperature, only 9.4 ms was acquired in the ^{13}C dimension. Although this was NUS-extrapolated to 18.8 ms, limited

resolution still hindered peak-picking in the ^{13}C dimension. In total, 131 total peaks were successfully peak-picked in NMRFAM-Sparky across all 35 spectra.

Prior to chemometric analyses, the peak tables, arranged in a manner similar to that described in Figure 1 from Section 3.1, were prepared in three forms, ^1H , ^{13}C weighted peaks, intensity values only, and Malmström distance (eq 8). PCA on the ^1H , ^{13}C weighted peaks afforded a plot that had very little discrimination between sample type (Figure 13A). Only the 100% ExoGal–NISTmAb was visually separated from all other spectra. Because the modifications to the NISTmAb molecule was only to the glycan residues as opposed to the amino acids, such a result was expected, as the previous report suggested that the spectral differences were from changes to protein dynamics, which would be read out in peak shape and intensity.¹⁹ If PCA is applied to the intensity alone at each peak position, a linear progression is observed in the plot from 0 to 100% ExoGal–NISTmAb (Figure 13B). If the Malmström distance is applied to the peak tables (panel C), the resulting PCA plot shows a less clear visual progression from 0 to 100% ExoGal–NISTmAb compared with panel B, consistent with the observation that the chemical shift value gave negligible discrimination to the sample type. Because of the poor performance of the PCA on peak tables, no cluster analyses were performed on the Figure 13 plots.

3.2.2. Analysis of the Total Spectral Matrix of Case Study #2. The total spectral matrix of the methyl region was extracted from each ^1H , ^{13}C spectrum in a manner similar to Figure 7 from Section 3.1. PCA was then performed with and without the 5% ExoGal sample and both with and without column centering (Figure 14A–C). In panel A, the 5% ExoGal cluster clearly has a great degree of overlap with 0 and 10% ExoGal clusters. However, if 5% ExoGal data are removed, the

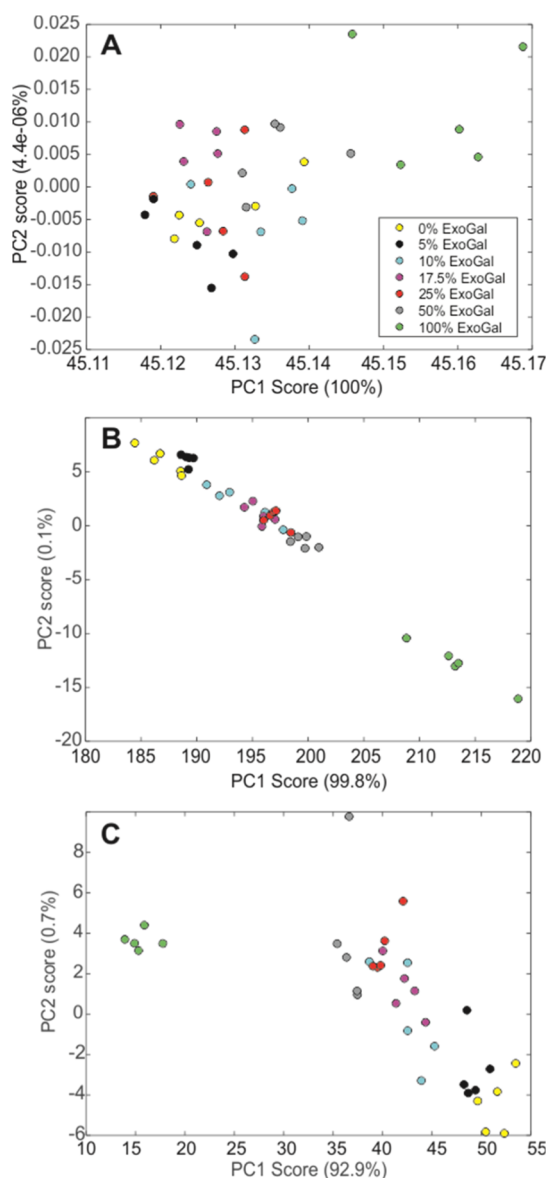


Figure 13. PCA plots from ^{13}C , ^{1}H methyl cross peaks from the blended ExoGal/native NISTmAb collected at 900 MHz and 50 °C. (A) ^{1}H , ^{13}C weighted peaks; (B) intensity values only from each cross peak position; (C) Malmström distance.

remaining sample types form distinct minimally overlapped clusters (panel B). For clarity, further analyses of the total spectral matrix of the blended samples will not include the 5% ExoGal spectra.

Several data pretreatment routines were applied to the 1D intensity vectors in order to evaluate their effect on the resulting PCA results. As a first attempt, subtraction of the column-centered means did not improve the cluster separation (panel C), consistent with the observation that traditional data centering is sub-optimal for NMR data. Second, if each pixel intensity is normalized to the average intensity of each pixel from all five spectra of the NISTmAb sample type, a suboptimal plot similar to panel C is observed (not shown). Last, literature reports suggest that binning the data prior to PCA may enhance clustering.⁵² To test this, all spectra were binned in the ^1H dimension separately to 0.01, 0.05, and 0.10 ppm. PCA on each of these data treatments afforded plots with

worsening cluster separation. One representative plot is shown in Figure 14D with the 0.05 ppm ^1H binning.

To assess the clusters in Figure 14, a cluster evaluation was performed. However, many of the metrics tested in Section 3.1.5 were found to afford unsatisfactory results. In particular, the Dunn index (eq 11) can give uncharacteristically low values if one or more clusters exhibit wide dispersion due to the “max” term in the denominator.^{47,48} Further, other metrics fail if the magnitude of the PCs are different primarily due to the raw summation of distances. This in particular affects silhouette values. The PC with the greatest magnitude will dominate the silhouette value, even if there is clear cluster discrimination from subsequent PCs. However, when the mean Euclidian distance from the centroid of each cluster is computed, cluster performance can be clearly evaluated (Figure 15). Predata treatments of normalization, centering, or direct PCA on the data affords comparable clusters. However, the degradation of cluster performance is clearly seen from 0.01 to 0.1 ppm ^1H binning. While these data pretreatments were not exhaustive, it appears that direct PCA on the matrix of intensity vectors may be preferred.

As mentioned in Section 3.1, an additional benefit afforded from direct PCA is that spectral loading plots can be computed so that the spectral changes can be visualized (Figure 16). The first PC affords the average spectrum from the entire data package. The second PC encodes the majority of the significant spectral changes. In this case study, intensity changes with only negligible chemical shift perturbations are observed across the majority of the spectral loading plot. This observation is consistent the lack of cluster separation observed from peak tables.

4. CONCLUSIONS

Although the NMR chemical shift is an intrinsic and truly robust parameter for fingerprinting the HOS of biologics, the question has remained about best practices for inputting NMR spectral data into chemometric algorithms. Chemical shift information alone does indeed offer some distinct advantages. The frequency position of each resonance is invariant to experimental setup, pulse sequence, or magnetic field, as demonstrated by the multinational interlaboratory study.²⁵ Structural and chemical perturbations to the molecule typically influence the chemical environment around a group of resonances and thereby cause changes in chemical shift position. A shifting of a group of resonances therefore indicates an alteration in the HOS of the molecule.^{53–55} However, other peak parameters such as peak intensity and line shape can report on quaternary interactions and possible changes in molecular dynamics where the chemical shifts are otherwise unchanged. Controlling these other spectral parameters is difficult, as these peak parameters are correlated to the system hardware (e.g., amplifiers, gain settings), magnetic field, and sample concentration. Because of these difficulties, the initial analyses of the multinational interlaboratory data package focused on chemical shifts (i.e., peak positions), for which pretreatment of the peak tables afforded highly similar score plots that would allow facile analyses (Figure 3). Incorporation of additional intensity information in the peak tables only showed a degradation of cluster performance (Figures 4 and 5), as might be anticipated based on the study design. Similarly, when interlaboratory study data were inputted as total spectral matrix into PCA analysis workflows, the resulting score plot showed a

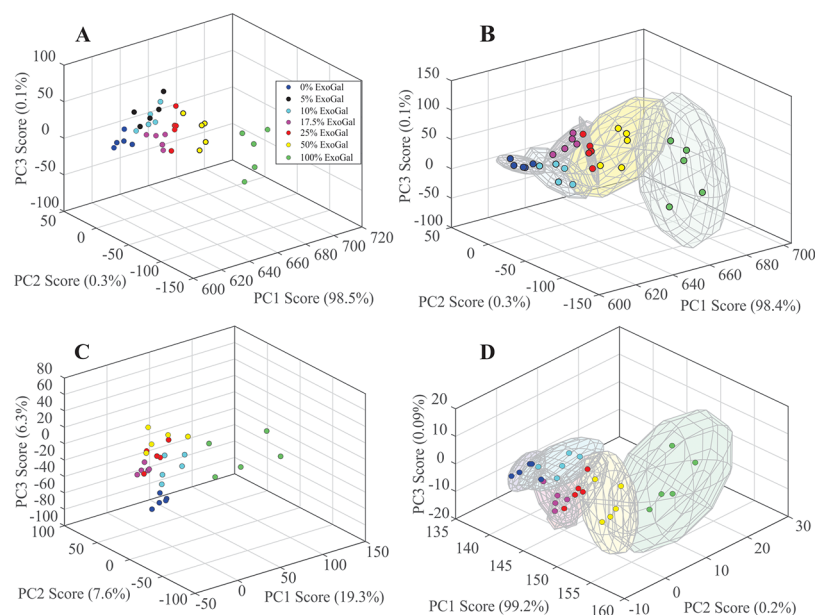


Figure 14. PCA plots from the total matrix of the methyl region of blended ExoGal/native NISTmAb collected at 900 MHz and 50 °C. All spectra were clustered manually according to sample blend. The error ellipsoids corresponded to the 95% confidence interval based on χ^2 probabilities. (A) All spectra, not centered; (B) all spectra except 5% ExoGal ($k = 6$), not centered; (C) $k = 6$, centered; (D) all 1D intensity vectors were binned to 0.05 ppm in the ^1H dimension, not centered. The PCA plots of the 0.01 or 0.10 ppm bins are not shown due to the visual similarity to panel (D). For best visualization, the points in panels (B,D) were pulled to the front of plot rather than leaving them embedded in the 3D ellipsoid. For panels (A,C), the error ellipsoids were removed due to the high degree of overlap.

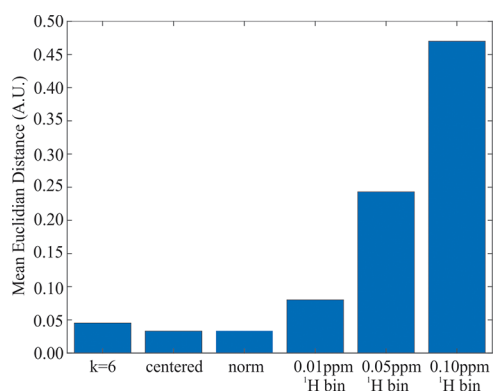


Figure 15. Mean Euclidian distance from the centroid of manual clusters, $k = 6$ without the 5% ExoGal spectra. The centering was performed by subtracting the column-centered means. Normalization was implemented by subtracting the average intensity of each pixel from the 100% NISTmAb spectra. For the final 3 bars, binning was performed in the ^1H dimension according to the label.

dependence on experimental setup and the magnetic field strength.

A limitation of using peak tables alone was highlighted by the second case study, which was designed to illustrate a situation in which HOS perturbations (e.g., glycan remodeling) only afforded changes in peak intensity rather than peak positions. Indeed, very little cluster discrimination was observed according to sample type from chemical shift information alone (Figure 13). Rather, distinct clusters were observed in the score plots from PCA of the total spectral matrix, with an LOD of approximately 10%, which is consistent with the previous report on a highly similar sample set (Figure 14).¹⁹

In a biopharmaceutical laboratory in which highly standardized methods are used, application of the 2D-NMR method will entail the use of one single qualified NMR system with strictly defined experimental parameters and protocols. Such use of a single, well-defined instrument setup and method can overcome the limitations of utilizing the total spectral matrix as input for chemometrics. Furthermore, analyses of the total

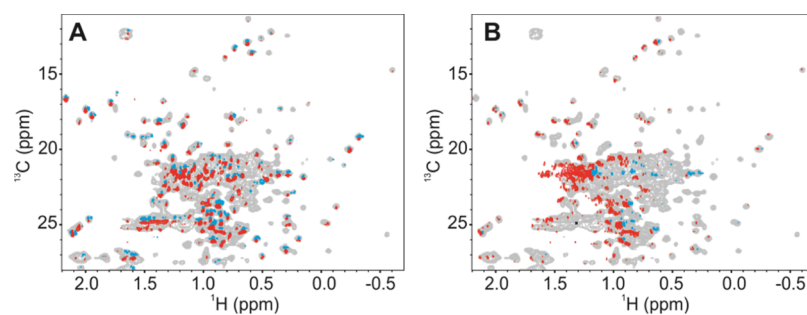


Figure 16. Spectral loading plot from all blended data with the 5% ExoGal removed. (A) PC2 on PC1; (B) PC3 on PC1. PC1 is in gray; positive contours are in blue and negative contours in red. The corresponding PCA score plot is found in Figure 14B.

spectral matrix using a consistent, well-defined data acquisition and processing methods could be automated for the nonexpert user and does not involve the potentially cumbersome and subjective task of peak-picking. While the multinational interlaboratory study established the repeatability and reproducibility of the 2D-NMR technique and suggested a method for data collection and analysis, the limitations in using the full matrix as data input did not represent a “real world” situation for characterization and supervision of a drug product. Application of the 2D NMR method across laboratories and magnetic field strengths might be required (e.g., transferring a qualified NMR method to another laboratory with a different field); however, in this situation, a bridging study could be performed to assure comparability.⁵⁶

Overall, this study has detailed some “best practices” for handling both peak positions and the total spectral matrix as input for chemometric algorithms. For most industrial applications, the total spectral matrix approach will likely be preferred when using a single, controlled experimental setup due to the ease of automation and limited intervention of an analyst. However, one could also envision applications in which peak positions may be preferred (e.g., comparison across multiple fields, situations where specific chemical shift changes are known to be correlated with product quality, etc.). As highlighted with these case studies, the exact implementation of chemometrics to NMR spectral data will depend on study design and will be chosen based on fit-for-purpose application for the specific product.

To date, only a few reports directly connect observed spectral changes to a functional change that could affect the safety and efficacy of a product.^{53–55} While more work stills need to be done to correlate an observed spectral perturbation to a clinically meaningful change, the spectral response to product variation will, to a large degree, need to be determined for a specific product. As such, analyses with the total spectra matrix from data acquired with a well-controlled experimental setup could be widely adapted for confident, detailed characterization of HOS across all stages of product development.

AUTHOR INFORMATION

Corresponding Author

Robert G. Brinson — Institute for Bioscience and Biotechnology Research, National Institute of Standards and Technology, The University of Maryland, Rockville, Maryland 20850, United States; orcid.org/0000-0001-5424-990X;
Email: robert.brinson@nist.gov

Authors

Luke W. Arbogast — Institute for Bioscience and Biotechnology Research, National Institute of Standards and Technology, The University of Maryland, Rockville, Maryland 20850, United States

John P. Marino — Institute for Bioscience and Biotechnology Research, National Institute of Standards and Technology, The University of Maryland, Rockville, Maryland 20850, United States

Frank Delaglio — Institute for Bioscience and Biotechnology Research, National Institute of Standards and Technology, The University of Maryland, Rockville, Maryland 20850, United States

Complete contact information is available at:
<https://pubs.acs.org/10.1021/acs.jcim.0c00081>

Notes

The authors declare no competing financial interest. Certain commercial equipment, instruments, and materials are identified in this paper in order to specify the experimental procedure. Such identification does not imply recommendation or endorsement by the National Institute of Standards and Technology, nor does it imply that the material or equipment identified is necessarily the best available for the purpose.

ACKNOWLEDGMENTS

The authors acknowledge the financial support from the NIST Biomanufacturing Program. The authors additionally acknowledge Anthony Kearsley and Ryan Evans for helpful discussions.

REFERENCES

- (1) Holmes, E.; Antti, H. Chemometric Contributions to the Evolution of Metabonomics: Mathematical Solutions to Characterising and Interpreting Complex Biological NMR Spectra. *Analyst* **2002**, *127*, 1549–1557.
- (2) McKenzie, J. S.; Donarski, J. A.; Wilson, J. C.; Charlton, A. J. Analysis of Complex Mixtures Using High-resolution Nuclear Magnetic Resonance Spectroscopy and Chemometrics. *Prog. Nucl. Magn. Reson. Spectrosc.* **2011**, *59*, 336–359.
- (3) Gómez-Caravaca, A. M.; Maggio, R. M.; Cerretani, L. Chemometric Applications to Assess Quality and Critical Parameters of Virgin and Extra-virgin Olive Oil. A Review. *Anal. Chim. Acta* **2016**, *913*, 1–21.
- (4) Pedersen, H. T.; Dyrby, M.; Engelsen, S. B.; Bro, R. Application of Multi-Way Analysis to 2D NMR Data. In *Annual Reports of NMR Spectroscopy*; Webb, G. A., Ed.; Elsevier: New York, 2006; Vol. 59, pp 207–233.
- (5) Robinette, S. L.; Brüschweiler, R.; Schroeder, F. C.; Edison, A. S. NMR in Metabolomics and Natural Products Research: Two Sides of the Same Coin. *Acc. Chem. Res.* **2012**, *45*, 288–297.
- (6) Cembran, A.; Kim, J.; Gao, J.; Veglia, G. NMR Mapping of Protein Conformational Landscapes Using Coordinated Behavior of Chemical Shifts upon Ligand Binding. *Phys. Chem. Chem. Phys.* **2014**, *16*, 6508–6518.
- (7) Xu, J.; Van Doren, S. R. Binding Isotherms and Time Courses Readily from Magnetic Resonance. *Anal. Chem.* **2016**, *88*, 8172–8178.
- (8) Namanja, A. T.; Xu, J.; Wu, H.; Sun, Q.; Upadhyay, A. K.; Sun, C.; Van Doren, S. R.; Petros, A. M. NMR-based Fragment Screening and Lead Discovery Accelerated by Principal Component Analysis. *J. Biomol. NMR* **2019**, *73*, 675–685.
- (9) Berglund, A.; Brorsson, A.-C.; Jonsson, B.-H.; Sethson, I. The Equilibrium Unfolding of MerP Characterized by Multivariate Analysis of 2D NMR Data. *J. Magn. Reson.* **2005**, *172*, 24–30.
- (10) Sakurai, K.; Goto, Y. Principal Component Analysis of the pH-dependent Conformational Transitions of Bovine Beta-lactoglobulin Monitored by Heteronuclear NMR. *Proc. Natl. Acad. Sci. U.S.A.* **2007**, *104*, 15346–15351.
- (11) Boulton, S.; Akimoto, M.; Selvaratnam, R.; Bashiri, A.; Melacini, G. A Tool Set to Map Allosteric Networks Through the NMR Chemical Shift Covariance Analysis. *Sci. Rep.* **2014**, *4*, 7306.
- (12) Župerl, Š.; Pristovšek, P.; Menart, V.; Gaberc-Porekar, V.; Novič, M. Chemometric Approach in Quantification of Structural Identity/Similarity of Proteins in Biopharmaceuticals. *J. Chem. Inf. Model.* **2007**, *47*, 737–743.
- (13) Amezcua, C. A.; Szabo, C. M. Assessment of Higher Order Structure Comparability in Therapeutic Proteins Using Nuclear Magnetic Resonance Spectroscopy. *J. Pharm. Sci.* **2013**, *102*, 1724–1733.
- (14) Arbogast, L. W.; Brinson, R. G.; Formolo, T.; Hoopes, J. T.; Marino, J. P. 2D 1HN, 15N Correlated NMR Methods at Natural Abundance for Obtaining Structural Maps and Statistical Comparability of Monoclonal Antibodies. *Pharm. Res.* **2016**, *33*, 462–475.

- (15) Konuma, T.; Lee, Y.-H.; Goto, Y.; Sakurai, K. Principal Component Analysis of Chemical Shift Perturbation Data of a Multiple-ligand-binding System for Elucidation of Respective Binding Mechanism. *Proteins* **2013**, *81*, 107–118.
- (16) Collins, K. M.; Oregioni, A.; Robertson, L. E.; Kelly, G.; Ramos, A. Protein-RNA Specificity by High-throughput Principal Component Analysis of NMR Spectra. *Nucleic Acids Res.* **2015**, *43*, No. e41.
- (17) Ghasriani, H.; Hodgson, D. J.; Brinson, R. G.; McEwen, I.; Buhse, L. F.; Kozlowski, S.; Marino, J. P.; Aubin, Y.; Keire, D. A. Precision and Robustness of 2D-NMR for Structure Assessment of Filgrastim Biosimilars. *Nat. Biotechnol.* **2016**, *34*, 139–141.
- (18) Brinson, R. G.; Ghasriani, H.; Hodgson, D. J.; Adams, K. M.; McEwen, I.; Freedberg, D. I.; Chen, K.; Keire, D. A.; Aubin, Y.; Marino, J. P. Application of 2D-NMR with Room Temperature NMR Probes for the Assessment of the Higher Order Structure of Filgrastim. *J. Pharm. Biomed. Anal.* **2017**, *141*, 229–233.
- (19) Arbogast, L. W.; Delaglio, F.; Schiel, J. E.; Marino, J. P. Multivariate Analysis of Two-dimensional ^1H , ^{13}C Methyl NMR Spectra of Monoclonal Antibody Therapeutics to Facilitate Assessment of Higher Order Structure. *Anal. Chem.* **2017**, *89*, 11839–11845.
- (20) Japelj, B.; Ilc, G.; Marusic, J.; Sencar, J.; Kuzman, D.; Plavec, J. Biosimilar Structural Comparability Assessment by NMR: from Small Proteins to Monoclonal Antibodies. *Sci. Rep.* **2016**, *6*, 32201.
- (21) Chen, K.; Park, J.; Li, F.; Patil, S. M.; Keire, D. A. Chemometric Methods to Quantify 1D and 2D NMR Spectral Differences Among Similar Protein Therapeutics. *AAPS PharmSciTech* **2018**, *19*, 1011–1019.
- (22) Wang, D.; Park, J.; Patil, S. M.; Smith, C. J.; Leazer, J. L.; Keire, D. A.; Chen, K. An NMR-Based Similarity Metric for Higher Order Structure Quality Assessment Among U.S. Marketed Insulin Therapeutics. *J. Pharm. Sci.* **2020**, *109*, 1519–1528.
- (23) Orekhov, V. Y.; Ibragimov, I. V.; Billeter, M. MUNIN: A New Approach to Multi-dimensional NMR Spectra Interpretation. *J. Biomol. NMR* **2001**, *20*, 49–60.
- (24) Orekhov, V. Y.; Jaravine, V. A. Analysis of Non-uniformly Sampled Spectra with Multi-dimensional Decomposition. *Prog. Nucl. Magn. Reson. Spectrosc.* **2011**, *59*, 271–292.
- (25) Brinson, R. G.; Marino, J. P.; Delaglio, F.; Arbogast, L. W.; Evans, R. M.; Kearsley, A.; Gingras, G.; Ghasriani, H.; Aubin, Y.; Pierens, G. K.; Jia, X.; Mobli, M.; Grant, H. G.; Keizer, D. W.; Schweimer, K.; Stähle, J.; Widmalm, G.; Zartler, E. R.; Lawrence, C. W.; Reardon, P. N.; Cort, J. R.; Xu, P.; Ni, F.; Yanaka, S.; Kato, K.; Parnham, S. R.; Tsao, D.; Blomgren, A.; Rundlöf, T.; Trieloff, N.; Schmieder, P.; Ross, A.; Skidmore, K.; Chen, K.; Keire, D.; Freedberg, D. I.; Suter-Stahel, T.; Wider, G.; Ilc, G.; Plavec, J.; Bradley, S. A.; Baldisseri, D. M.; Sforça, M. L.; Zeri, A. C. d. M.; Wei, J. Y.; Szabo, C. M.; Amezcua, C. A.; Jordan, J. B.; Wikström, M. Enabling Adoption of 2D-NMR for the Higher Order Structure Assessment of Monoclonal Antibody Therapeutics. *MAbs* **2019**, *11*, 94–105.
- (26) Schiel, J. E.; Mire-Sluis, A.; Davis, D. Monoclonal Antibody Therapeutics: The Need for Biopharmaceutical Reference Materials. In *State-of-the-Art and Emerging Technologies for Therapeutic Monoclonal Antibody Characterization Volume 1. Monoclonal Antibody Therapeutics: Structure, Function, and Regulatory Space*; American Chemical Society, 2014; Vol. 1176, Chapter 1, pp 1–34.
- (27) Schiel, J. E.; Turner, A. The NISTmAb Reference Material 8671 Lifecycle Management and Quality Plan. *Anal. Bioanal. Chem.* **2018**, *410*, 2067–2078.
- (28) Delaglio, F.; Grzesiek, S.; Vuister, G. W.; Zhu, G.; Pfeifer, J.; Bax, A. NMRPipe: A Multidimensional Spectral Processing System Based on UNIX Pipes. *J. Biomol. NMR* **1995**, *6*, 277–293.
- (29) Lee, W.; Tonelli, M.; Markley, J. L. NMRFAM-SPARKY: Enhanced Software for Biomolecular NMR Spectroscopy. *Bioinformatics* **2015**, *31*, 1325–1327.
- (30) Wang, Y.; Jardetzky, O. Investigation of the Neighboring Residue Effects on Protein Chemical Shifts. *J. Am. Chem. Soc.* **2002**, *124*, 14075–14084.
- (31) Mechelke, M.; Habeck, M. A Probabilistic Model for Secondary Structure Prediction from Protein Chemical Shifts. *Proteins* **2013**, *81*, 984–993.
- (32) Han, B.; Liu, Y.; Ginzinger, S. W.; Wishart, D. S. SHIFTX2: Significantly Improved Protein Chemical Shift Prediction. *J. Biomol. NMR* **2011**, *50*, 43–57.
- (33) Berjanskii, M. V.; Wishart, D. S. Unraveling the Meaning of Chemical Shifts in Protein NMR. *Biochim. Biophys. Acta, Proteins Proteomics* **2017**, *1865*, 1564–1576.
- (34) Nerli, S.; McShan, A. C.; Sgourakis, N. G. Chemical Shift-based Methods in NMR Structure Determination. *Prog. Nucl. Magn. Reson. Spectrosc.* **2018**, *106–107*, 1–25.
- (35) van der Schot, G.; Zhang, Z.; Vernon, R.; Shen, Y.; Vranken, W. F.; Baker, D.; Bonvin, A. M. J. J.; Lange, O. F. Improving 3D structure prediction from chemical shift data. *J. Biomol. NMR* **2013**, *57*, 27–35.
- (36) Markley, J. L.; Bax, A.; Arata, Y.; Hilbers, C. W.; Kaptein, R.; Sykes, B. D.; Wright, P. E.; Wuthrich, K. Recommendations for the Presentation of NMR Structures of Proteins and Nucleic Acids. IUPAC-IUBMB-IUPAB Inter-Union Task Group on the Standardization of Data Bases of Protein and Nucleic Acid Structures Determined by NMR Spectroscopy. *Eur. J. Biochem.* **1998**, *256*, 1–15.
- (37) Maniara, G.; Rajamoorthi, K.; Rajan, S.; Stockton, G. W. Method Performance and Validation for Quantitative Analysis by ^1H and ^{31}P NMR Spectroscopy. Applications to Analytical Standards and Agricultural Chemicals. *Anal. Chem.* **1998**, *70*, 4921–4928.
- (38) Johnson, B. A. From Raw Data to Protein Backbone Chemical Shifts Using NMRFX Processing and NMRViewJ Analysis. *Methods Mol. Biol.* **2018**, *1688*, 257–310.
- (39) Williamson, M. P. Using Chemical Shift Perturbation to Characterise Ligand Binding. *Prog. Nucl. Magn. Reson. Spectrosc.* **2013**, *73*, 1–16.
- (40) Abdi, H.; Williams, L. J. Principal Component Analysis. *WIREs Comp. Stats.* **2010**, *2*, 433–459.
- (41) Aubin, Y.; Hodgson, D. J.; Thach, W. B.; Gingras, G.; Sauvé, S. Monitoring Effects of Excipients, Formulation Parameters and Mutations on the High Order Structure of Filgrastim by NMR. *Pharm. Res.* **2015**, *32*, 3365–3375.
- (42) Chae, Y. K.; Kim, S. H.; Nam, Y.-K. Application of Two-Dimensional NMR Spectroscopy to Metabotyping Laboratory Escherichia coli Strains. *Chem. Biodiversity* **2013**, *10*, 1816–1827.
- (43) Majumder, S.; DeMott, C. M.; Burz, D. S.; Shekhtman, A. Using Singular Value Decomposition to Characterize Protein-Protein Interactions by In-Cell NMR Spectroscopy. *Chembiochem* **2014**, *15*, 929–933.
- (44) Haxholm, G. W.; Petersen, B. O.; Malmström, J. Higher-Order Structure Characterization of Pharmaceutical Proteins by 2D Nuclear Magnetic Resonance Methyl Fingerprinting. *J. Pharm. Sci.* **2019**, *108*, 3029–3035.
- (45) Davies, D. L.; Bouldin, D. W. A Cluster Separation Measure. *IEEE Trans. Pattern Anal. Mach. Intell.* **1979**, *PAMI-1*, 224–227.
- (46) Kaufman, L.; Rousseeuw, P. J. *Finding Groups in Data: An Introduction to Cluster Analysis*; John Wiley & Sons, Inc: Hoboken, NJ, 2005.
- (47) Dunn, J. C. A Fuzzy Relative of the ISODATA Process and Its Use in Detecting Compact Well-Separated Clusters. *J. Cybern.* **1973**, *3*, 32–57.
- (48) Dunn, J. C. Well-Separated Clusters and Optimal Fuzzy Partitions. *J. Cybern.* **1974**, *4*, 95–104.
- (49) Arbogast, L. W.; Brinson, R. G.; Marino, J. P. Mapping Monoclonal Antibody Structure by 2D ^{13}C NMR at Natural Abundance. *Anal. Chem.* **2015**, *87*, 3556–3561.
- (50) Stoyanova, R.; Brown, T. R. NMR Spectral Quantitation by Principal Component Analysis. *NMR Biomed.* **2001**, *14*, 271–277.
- (51) Halouska, S.; Powers, R. Negative impact of noise on the principal component analysis of NMR data. *J. Magn. Reson.* **2006**, *178*, 88–95.
- (52) Alam, T. M.; Alam, M. K. Chemometric Analysis of NMR Spectroscopy: A Review. In *Annual Reports of NMR Spectroscopy*;

Webb, G., Ed.; Academic Press: Cambridge, MA, 2005; Vol. 54, pp 43–80.

(53) Bandi, S.; Singh, S. M.; Shah, D. D.; Upadhyay, V.; Mallela, K. M. G. 2D NMR Analysis of the Effect of Asparagine Deamidation Versus Methionine Oxidation on the Structure, Stability, Aggregation, and Function of a Therapeutic Protein. *Mol. Pharm.* **2019**, *16*, 4621–4635.

(54) Shah, D. D.; Zhang, J.; Hsieh, M.-c.; Sundaram, S.; Maity, H.; Mallela, K. M. G. Effect of Peroxide- Versus Alkoxy-Induced Chemical Oxidation on the Structure, Stability, Aggregation, and Function of a Therapeutic Monoclonal Antibody. *J. Pharm. Sci.* **2018**, *107*, 2789–2803.

(55) Majumder, S.; Saati, A.; Philip, S.; Liu, L. L.; Stephens, E.; Rouse, J. C.; Ignatius, A. A. Utility of High Resolution NMR Methods to Probe the Impact of Chemical Modifications on Higher Order Structure of Monoclonal Antibodies in Relation to Antigen Binding. *Pharm. Res.* **2019**, *36*, 130.

(56) European Medicines Agency. *ICH Q5E Biotechnological/Biological Products Subject to Changes in Their Manufacturing Process: Comparability of Biotechnological/Biological Products*, London, UK, 2005, CPMP/ICH/5721/03, step 5.